EARTH SCIENCES
RESEARCH JOURNAL
Earth Sci. Res. J. Vol. 28, No. 4 (December, 2024): 447 - 460

UNIVERSIDAD NACIONAL DE COLOMBIA

EARTHQUAKE ENGINEERING

Estimation of the date and magnitude of impending massive earthquakes using the integration of precursors obtainable from remote sensing data

Mohammad Mahdi Khoshgoftar*, Mohammad Reza Saradjian
School of Surveying and Geospatial Engineering, College of Engineering, University of Tehran, Tehran, Iran
*Corresponding author: mm.khoshgoftaar@ut.ac.ir

ABSTRACT

A single precursor is not usually an accurate, precise, and adequate measure to predict earthquake parameters. Therefore, it is more appropriate to combine multiple precursors and exploit parameters extracted from them to reduce the uncertainty of the prediction. The assumption in this study is based on the fact that most Earthquakes happen in active fault zones. The study is about the estimation of Earthquake parameters such as date and magnitude. In this study, remote sensing observations (such as electron and ion density, electron temperature, Total Electron Content (TEC), Land Surface Temperature (LST), Sea Surface Temperature (SST), Aerosol Optical Depth (AOD), and Surface Latent Heat Flux (SLHF)) in different modalities acquired several days before impending earthquakes have been investigated to extract earthquake parameters. In this study, three methods: median, support vector regression (SVR), and random forest (RF) have been used to detect anomalies. Then, by estimating the amount of anomaly deviation from the normal state, the magnitude of the impending earthquake is estimated. The final earthquake parameters (such as date and magnitude) can be obtained by integrating the earthquake parameters extracted from different earthquake precursors using the mean square error (MSE) method.

Keywords: Earthquake, anomaly detection, remote sensing, support vector machine, random forest

Estimación del momento y la magnitud de los terremotos masivos inminentes a través de la integración de precursores obtenidos a través de información de detección remota

RESUMEN

Un solo precursor no es usualmente una medida exacta, precisa y adecuada para predecir los parámetros de un terremoto. Además, es más apropiado combinar múltiples precursores e identificar sus propios parámetros para reducir la incertidumbre de la predicción. El supuesto de este trabajo está basado en que la mayoría de terremotos ocurren en zonas de fallas activas. Este estudio se basa en la estimación de los parámetros de terremoto como momento y magnitud. En este trabajo se investigaron las observaciones de detección remota en diferentes modalidades (tales como densidad de iones y electrones, temperatura de electrones, contenido total de electrones, temperatura de la superficie terrestre, temperatura de la superficie marina, profundidad óptica del aerosol y flujo de calor latente), adquiridas varios días antes de los terremotos inminentes, para extraer los parámetros del terremoto. Se usaron tres métodos para detectar las anomalías: mediana, regresión de vectores de soporte, y bosque aleatorio. Luego se estimó la magnitud de los terremotos inminentes al estimar la medida de la desviación de la anomalía. Los parámetros finales del terremoto (como momento y magnitud) se pueden obtener al integrar los parámetros de terremoto extraídos de diferentes precursores de terremoto al usar el método del error cuadrático medio.

Palabras clave: terremoto; detección de anomalías; detección remota; máquina de vectores de soporte; bosque aleatorio

Record
Manuscript received: 02/10/2022
Accepted for publication: 10/12/2024

How to cite item:
Khoshgoftar, M. M., & Saradjian M. R. (2024). Estimation of the date and magnitude of impending massive earthquakes using the integration of precursors obtainable from remote sensing data. *Earth Sciences Research Journal, 28*(4), 447-460. https://doi.org/10.15446/esrj.v28n4.105079

ISSN 1794-6190 e-ISSN 2339-3459
https://doi.org/10.15446/esrj.v28n4.105079

1. Introduction

When an earthquake is happening, energy transmission is generated due to the destructive effects of the earthquake on the environment. The occurrence of these changes before and/or after the earthquake may have various physical and chemical effects on the lithosphere, atmosphere, and ionosphere, making the earthquake more accurately predictable. The abnormal variations in lithospheric, atmospheric, and ionosphere parameters are taken as "earthquake precursors". They serve as alarms for impending earthquakes. Many studies have been carried out on earthquake predictions using precursors in the lithosphere, atmosphere, and ionosphere. The problem arises when some of these major abnormalities do not appear during an earthquake. There are several studies based on the observation of the seismic Lithosphere Atmosphere Ionosphere Coupling (LAIC) anomalies which confirm that the anomalies begin several days before the earthquake and remain a few days after. None of the earthquake precursors can be used alone as an accurate and independent parameter for estimating earthquake parameters without generating some level of uncertainty. Hence, it is necessary to integrate different types of earthquake predictors or precursors. By integrating a variety of earthquake parameters extracted from different precursors, a more accurate and suitable estimation of the final earthquake parameters may be obtained.

Recent advances in remote sensing and Earth observation technology have facilitated monitoring the ionosphere, the atmosphere, and the Earth's surface using various sensors. Nowadays, researchers investigate the factors and indications of earthquakes in more practical and efficient ways. The most important earthquake precursors relevant to ionospheric anomalies recently studied are changes in ion density, ion temperature, electron density, and electron temperature provided by DEMETER satellite data (Berthelier et al., 2006; Lebreton et al., 2006; Parrot et al., 2006; Li and Parrot 2012; Li and Parrot 2013; Tao et al., 2017; Ibanga et al., 2018; Li and Parrot 2018). Ionospheric anomaly studies also include changes in total electron content (TEC) obtained from global positioning receivers (GPS) (Liu et al., 2004; Akhoondzadeh 2013; Tao et al., 2017; Akhoondzadeh et al., 2019). Regarding the Earth's surface, another useful precursor is thermal anomaly obtainable from land surface temperature (LST) (Ouzounov and Freund 2004; Ouzounov et al., 2006; Tronin 2006; Panda et al., 2007; Saraf et al., 2008; Blackett et al., 2011; Zoran 2012; Akhoondzadeh 2013; Bhardwaj et al., 2017a; Bhardwaj et al., 2017b, Chen et al., 2020; Jiao and Shan 2021), and from sea surface temperature (SST) (Dziak et al., 2003; Ouzounov et al., 2006; Freund et al., 2009). Other useful precursors are outgoing longwave radiation (OLR) (Ouzounov et al., 2007; Rawatet et al., 2011; Eleftheriou et al., 2016), surface latent heat flux (SLHF) (Dey and Singh 2003; Cervone et al., 2004; Cervone et al., 2006; Pulinets et al., 2006; Pulinets and Ouzounov 2011; Zhang et al., 2013; MansouriDaneshvar et al., 2014; Qin et al., 2014), and atmospheric anomalies in the form of aerosol optical depth (AOD) (Freund et al. 2009; Akhoondzadeh, 2015; Ganguly, 2016; Akhoondzadeh, 2018; Akhoondzadeh et al., 2019).

2. Data

According to the objective of this study, the data used have been chosen from multiple sources, which are as follows:

DEMETER data

The French microsatellite DEMETER was launched in June 2004, and its scientific mission stopped on December 9, 2010. The data provided by DEMETER is used to investigate ionospheric disturbances due to seismic activity (Parrot et al., 2006). The DEMETER satellite collected its ionospheric parameters related to seismic activities using five sensors. The sensors are Instrument Champ Eletrique (ICE), Instrument Magnetic Search Coil (IMSC), Instrument Detecteur de Partcules (IDP), Instrument Analyseur Plasma (IAP), and Instrument Sonde de Longmuir (ISL). In this study, ion density (cm-3) and ion temperature (K), as well as electron density(cm^{-3}) and electron temperature(K) data were collected from ISL and IAP sensors. DEMETER satellite data is available via: http://demeter.cnrs-orleans.fr/.

TEC data

The most popular product to analyse the ionosphere state is the global ionosphere maps (GIM) of the Total Electron content (TEC) provided by NASA (National Aeronautics and Space Administration) in the IONEX format. The GIM-TEC covers ± 87.5 of latitude and ± 180 of longitude with a spatial resolution of 2.5 and 5.0, respectively, and a cadence of 2h. In this study, the TEC variations according to the closest node to the epicentre of the earthquakes have been analysed. The GIM-TEC map is obtained from the website https://cddis.nasa.gov/archive/gnss/products/ionex/.

MODIS data

Two products of Moderate Resolution Imaging Spectroradiometer (MODIS) satellite, i.e., Land Surface Temperature (LST) and Aerosol Optical Depth (AOD) data were used in this study. Both the day/night-time LST images provided by NASA (http://modis.gsfc.nasa.gov/data) were processed. The MODIS Terra and Aqua daily level-3 aerosol product, which is produced by the Dark Target and Deep Blue algorithms and is called ''Aerosol Optical Depth at 550 nm", is available vie: https://giovanni.gsfc.nasa.gov/giovanni/.

AVHRR data

Two products of AVHRR (Advanced Very High Resolution Radiometer) including Sea Surface Temperature (SST) and Surface Latent Heat Flux (SLHF) data have been used in this study. Sea surface temperature (SST) anomaly can be related to near coastal seismic activity (Ouzounov and Freund, 2004), but conditions and currents can strongly affect SST. Due to a large thermal inertia of the seawater, its temperature changes more slowly; therefore, in the case of the SST anomalies, some mechanisms of LST anomalies are not applicable (Jiao et al., 2018). The NOAA 0.25° daily Optimum Interpolation Sea Surface Temperature (OISST) is an analysis constructed by combining observations from different platforms (satellites, ships, buoys) on a regular global grid. A spatially complete SST map is produced by interpolating to fill in gaps. The SST products are available via:https://psl.noaa.gov/data/gridded/data.noaa.oisst.v2.highres.html.

SLHF is (Wm^{-2}) the heat flux absorbed or released by the phase transition (i.e., condensation, evaporation, and melting) of water from the Earth's surface to the atmosphere (Jiao et al., 2018). SLHF is one of the important components of Earth's surface energy budget, which is mainly affected by the atmospheric relative humidity, wind speed, surface temperature, and season (Jiao et al., 2018). Due to the underground fluid movement and the interaction among the underground, surface, and atmosphere, the SLHF anomaly that occurs prior to earthquakes is considered (Alvan et al., 2013). The SLHF products are available via:https://psl.noaa.gov/data/gridded/data.ncep.reanalysis.html.

Geomagnetic indices

The ionospheric parameters measured by satellite are mainly influenced by the geomagnetic storms and geomagnetic field disturbances, particularly in the equatorial and polar regions. However, in the case of an impending Earthquake, it may be affected further more in the form of anomaly. Such anomalies should also be removed. In order to distinguish anomalies caused by seismic activity from anomalies created by geomagnetic and solar activities, the geomagnetic and solar indices i.e. Dst, Kp, Ap, and F10.7 acquired from Space Physics Data Facility (SPDF) have been utilized in this study. In conditions where the quiet solar geomagnetic is established (i.e. $Kp < 2.5$, $-20\ nT < Dst < 20\ nT$ and $F10.7 < 120$ SFU) the situation will be regarded as normal. However, if unusual changes are seen in the ionospheric data, it can be considered due to seismic activity. The geomagnetic and solar indices are available through NOAA (https://www.ngdc.noaa.gov/stp/stp.html).

3. Method

Anomaly detection method

Anomaly detection is the process of identifying unexpected items or events in data sets, which differ from the norm. Anomaly detection has two basic assumptions: 1) anomalies only occur very rarely in the data, and 2) their features differ from the normal instances significantly. In order to detect anomalies in each set of time series data from remotely sensed precursors, identification of the normal behaviour of the phenomenon is necessary.

3.1a. Normal behavior modeling

In order to model time series behaviour, two common machine learning methods namely the Support Vector Regression (SVR) and Random Forest (RF) have been used in this study.

In SVR-based regression solutions, the input vectors are mapped into a higher-dimensional feature space, then by employing a linear regression in the feature space, the input vectors are separated as far apart as possible. In this study, which is operating in a large space, a kernel function is used (Khosravi et al., 2017).

Random forest algorithm which is a nonparametric machine learning ensemble method, is an extended version of CART (Classification and Regression Trees) model proposed by Breiman (2001). It is based on the information combination method in which a large number of decision trees are generated and then the results of all the trees are combined for prediction (Cutler et al. 2007). The RF is the multitude of regression trees which performs based on the variance of the data (Liaw and Wiener, 2002).

3.1b. Anomaly detection

In order to detect anomalies, a reasonable range for regular variations in the time series data should be specified. Signals with normal behaviour fluctuate inside both the upper and lower bounds. Signals outside the boundaries will be detected as anomalies. In this study, the median and interquartile method is used to determine the upper and lower bounds (Liu et al., 2004).

The upper and lower bounds are determined using the following Eq. (1):

$$\begin{cases} x_{\text{low}} = m - k \times iqr \\ x_{high} = m + k \times iqr \end{cases} \quad (1)$$

Where x_{low}, x_{high}, m and iqr are respectively the lower bound, upper bound, median value and interquartile range of x. If the signal lies within the range of the upper and lower bounds, the behaviour of the signal is considered as normal. To determine the intensity of abnormal behaviour of the signal, the parameter D_x as deviation of x is calculated by Eq. (2):

$$x_{\text{low}} < x < x_{\text{high}} \Rightarrow -k < D_x = \frac{x-m}{iqr} < k \quad (2)$$

If the absolute value of the parameter D_x is greater than k (i.e. $|D_x| > k$), the behaviour of the parameter is regarded as anomalous. Also, the percentage of parameter deviation from the natural state can be calculated using the Eq. (3) (Saradjian and Akhoondzadeh, 2011):

$$P = \pm 100 \times ((|D_x| - k)/k) \quad (3)$$

Preliminary parameters estimation

The Earthquake parameters are preliminarily estimated for each individual precursor. The D_x value obtained from the previous step is quite suitable parameter for calculating Earthquake magnitude. Saradjian and Akhoondzadeh (2011) showed the relationship between this parameter and the Earthquake magnitude that can be extracted from Table (1). Although the selection of D_x and its correspondence with magnitude ranges was investigated previously in another study (Saradjian and Akhoondzadeh, 2011), but it was investigated again in this study and verified.

Table 1. Earthquake magnitude estimation (Saradjian and Akhoondzadeh, 2011)

Dx value	Earthquake magnitude
$D_x \leq 1$	$\boldsymbol{Mw \leq 6}$
$1 < D_x \leq 2$	$\boldsymbol{6 < Mw \leq 7}$
$2 < D_x \leq 3$	$\boldsymbol{7 < Mw \leq 8}$
$3 < D_x$	$\boldsymbol{8 < Mw}$

Also, according to the day when the anomaly is observed, an impending Earthquake's approximate date can be estimated. Based on observations so far, as an average, a 15-day interval in ionospheric and atmospheric precursors, and as an average, a 16-day interval in thermal precursors from the anomaly observation till earthquake day is considered (Saradjian and Akhoondzadeh, 2011). Although the periods of 15 or 16 days were estimated previously by other researchers (Ouzounov and Freund, 2004; Pulinets et al, 2006; Jiao et al., 2018; Saradjian and Akhoondzadeh, 2011), but it was investigated again in this study and verified.

Finalizing parameters estimation method

After the earthquake parameters (i.e. date and magnitude) are estimated through various precursors using the preliminarily Earthquake parameters estimation, the final value of parameters of the earthquake can be estimated by combining their results using MSE method. In MSE method, the date and magnitude of an earthquake is calculated by Eq. (4) (Wackerly et. al., 2008):

$$MSE = V + (x - M)^2 \quad (4)$$

where V and M are variance and median for the predicted upper and lower limits for the date and magnitude of the earthquake are calculated separately for all precursors. Finally, any parameter that has a minimum value of MSE is considered as the final parameter of the earthquake. This equation is applied when MSE is used as an estimator. Since input to MSE is not a physical quantity the difference in the type of precursors has no effect.

4. Case Studies and Results

Four major earthquakes with Magnitude Mw > 6 have been investigated in this study. These earthquakes occurred in Samoa Islands, Sichuan (China), Kermanshah and Bam (Iran). The characteristics of these earthquakes have been presented in Table 2. The ionospheric parameters obtained from the DEMETER has been studied and analysed over the relevant periods of time for each earthquake for areas selected according to Dobrovolsky Formula $R = 10^{0.43M}$ which relates the size of affected area to the magnitude of the earthquake (Dobrovolsky et al., 1979). The rest of the time series data for other precursors have been acquired for the relevant periods of time for areas of about 5×5 degrees in size around each epicentre. All time series data were provided for the period of 100 days and in some cases more than 100 days.

Table 2. Characteristics of earthquakes investigated in this study (http://earthquake.usgs.gov/)

Case Study	Date	Time (UTC)	Latitude	Longitude	Mw	Depth (km)
Kermanshah, Iran	2017-11-12	18:18:17	34.91 E	45.96 N	7.3	19
Samoa Islands	2009-09-29	17:48:10	15.59 W	172.10 S	8.1	18
Sichuan, China	2008-05-12	06:28:01	31.00 E	103.32 N	7.9	19
Bam, Iran	2003-12-26	01:56:52	29.00 E	58.31 N	6.6	10

Kermanshah earthquake

In the case study of Kermanshah Earthquake, all-time series data were provided for the period of 1 August to 27 November 2017. The TEC anomaly associated with Kermanshah earthquake was observed on November 4 (Table 3). By observing this anomaly, it can be concluded that an earthquake with magnitude ranging from 7 to 8 Mw between November 5 and 19, 2017 would have happened (Figure 1d).

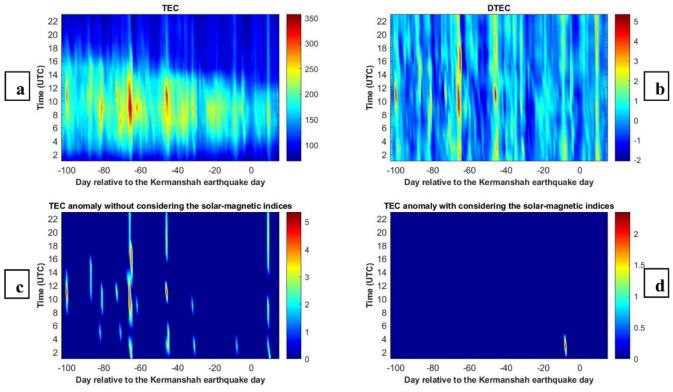

Figure 1. Results of TEC Analysis using median for Kermanshah earthquake. The earthquake time is indicated by an asterisk. (a) TEC variations, (b) DTEC, (c) Detected anomalies without considering the solar-magnetic indices, (d) Detected anomalies with considering the solar-magnetic indices.

By investigating the Aqua night-time LST (°C) anomalies, the maximum value of 3.04°C October 28 indicates an earthquake between October 29 and November 13 with Mw>8 would have happened (Figure 2a).

The anomaly observed in the AOD data obtained from the Aqua sensor, with a maximum of 452.78% on October 30, 2017, indicates an impending earthquake with *Mw*>8 between October 31 and November 15 (Figure 2b). Also, the estimated earthquake magnitude for the observed anomaly on November 2, 2017 related to the AOD precursor obtained from the Terra sensor would be greater than 8*Mw* (Figure 2c).

By investigating the changes in SLHF, a sharp increase of 126.97%, 213.64% have been observed on 3 and 4 October, respectively (Figure 2(d)). Due to these anomalies, it can be predicted that an earthquake with magnitude more than 8 Mw will occur in the region. Another sharp increase of 204.36% has been observed on 30 October, it can be indicating an earthquake with Mw>8 between October 31 and November 15 would have happened.

The results obtained by SVR and Random Forest methods can be found in tables 4 and 5, respectively.

In the case study of Kermanshah, the earthquake parameters deduced based on median from the different precursors using the MSE method indicate that an earthquake would occur between November 1 and 16 with a magnitude more than 8 Mw (Table 15). Also by using MSE method for the obtained results from both SVR and RF methods, the predicted magnitude of earthquake will be, respectively, from 7 to 8 Mw between November 1 and 16, 2017 and from 7 to 8 Mw between October 29 and November 16, 2017 (Table 15).

Table 3. List of anomalies obtained from different precursors of Kermanshah earthquake using Median method

Precursor	Date of observed anomaly	Prediction of earthquake date	Deviation value (Dx)	Prediction of earthquake magnitude (Mw)
TEC	4 Nov (UTC=04:00)	5 Nov-19 Nov	2.35	7<Mw<8
LST Aqua (Night Time)	2 Nov	3 Nov-18 Nov	2.92	7<Mw<8
	28 Oct	29 oct-13 Nov	3.04	Mw>8
Aerosol Optical Depth (Aqua)	2 Nov	3 Nov-18 Nov	2.95	7<Mw<8
	30 Oct	31 Oct-15 Nov	12.16	Mw>8
Aerosol Optical Depth (Terra)	2 Nov	3 Nov-18 Nov	3.96	Mw>8
SLHF	7 Nov	8 Nov-23 Nov	2.70	7<Mw<8
	6 Nov	7 Nov-22 Nov	3.05	Mw>8
	5 Nov	6 Nov-21 Nov	3.61	Mw>8
	4 Nov	5 Nov-20 Nov	5.10	Mw>8
	3 Nov	4 Nov-19 Nov	4.15	Mw>8
	30 Oct	31 Oct-15 Nov	6.70	Mw>8
	5 Oct	6 Oct-21 Oct	2.68	7<Mw<8
	4 Oct	5 Oct-20 Oct	6.90	Mw>8
	3 Oct	4 Oct-19 Oct	4.99	Mw>8

Table 4. List of anomalies obtained from different precursors of Kermanshah earthquake using SVR method

Precursor	Date of observed anomaly	Prediction of earthquake date	Deviation value (Dx)	Prediction of earthquake magnitude (Mw)
TEC	27 Oct (UTC=22:00)	28 Oct-11 Nov	2.06	7<Mw<8
	27 Oct (UTC=12:00)	28 Oct-11 Nov	2.11	7<Mw<8
	27 Oct (UTC=08:00)	28 Oct-11 Nov	2.01	7<Mw<8
LST Aqua (Night Time)	2 Nov	3 Nov-18 Nov	2.39	7<Mw<8
Aerosol Optical Depth (Aqua)	31 Oct	1 Nov-16 Nov	5.82	Mw>8
Aerosol Optical Depth (Terra)	2 Nov	3 Nov-18 Nov	3.94	Mw>8
SLHF	3 Nov	4 Nov-19 Nov	2.06	7<Mw<8
	31 Oct	1 Nov-16 Nov	-2.24	7<Mw<8
	30 Oct	31 Oct-15 Nov	3.11	Mw>8

Table 5. List of anomalies obtained from different precursors of Kermanshah earthquake using Random Forest method

Precursor	Date of observed anomaly	Prediction of earthquake date	Deviation value (Dx)	Prediction of earthquake magnitude (Mw)
TEC	28 Oct (UTC=04:00)	29 Oct-12 Nov	2.06	7<Mw<8
	27 Oct (UTC=22:00)	28 Oct-11 Nov	2.14	7<Mw<8
	27 Oct (UTC=12:00)	28 Oct-11 Nov	2.87	7<Mw<8
	27 Oct (UTC=08:00)	28 Oct-11 Nov	2.36	7<Mw<8
	27 Oct (UTC=04:00)	28 Oct-11 Nov	2.11	7<Mw<8
LST Aqua (Night Time)	2 Nov	3 Nov-18 Nov	2.57	7<Mw<8
Aerosol Optical Depth (Aqua)	31 Oct	1 Nov-16 Nov	5.81	Mw>8
Aerosol Optical Depth (Terra)	2 Nov	3 Nov-18 Nov	4.09	Mw>8
SLHF	30 Oct	31 Oct-15 Nov	2.71	7<Mw<8

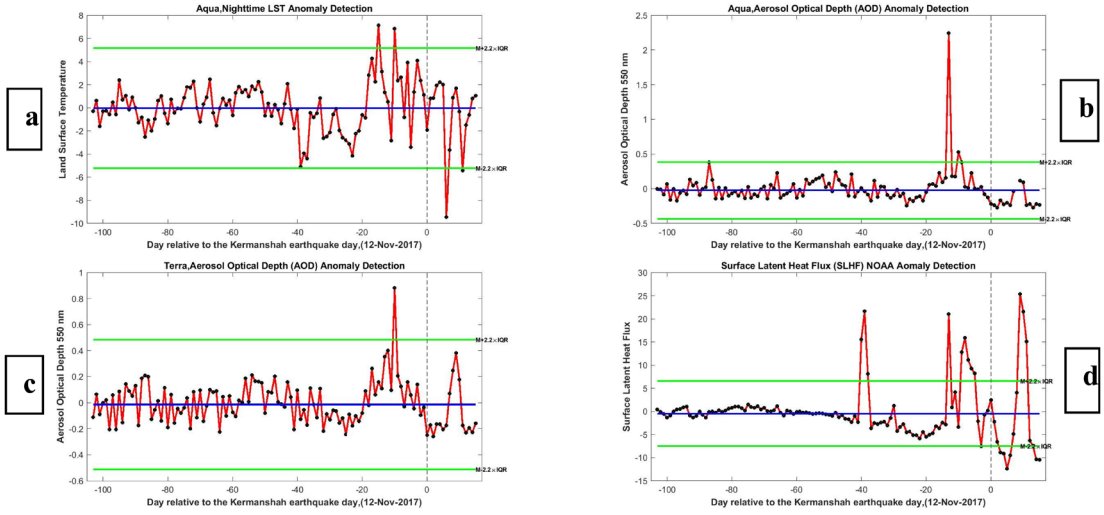

Figure 2. Results of (a) Night-time LST data (Aqua, MODIS), (b) AOD (Aqua, MODIS), (c) AOD (Terra, MODIS), (d) SLHF (NOAA), analysis using median method for Kermanshah earthquake. The earthquake day is displayed as a vertical dotted line. The green horizontal lines indicate the higher and lower bounds. The blue line indicates the median value.

Samoa earthquake

For the Samoa earthquake, the time series data of precursors were provided for the period of 1 June to 15 October 2009. TEC anomaly fluctuations began on September 18. The estimated magnitude of the Earthquake for this anomaly would have more than 8 Mw happening between September 19 and October 3. Anomalies have also been observed on September 25 and 28, 2009 implying that an Earthquake with magnitude greater than $Mw = 8.0$ would be expected to happen (Figure 3(d)).

The data on the changes in total ion density, electron and ion density and electron temperature recorded by DEMETER IAP and ISL sensors for Samoa Earthquake are given in Table 6. The data were recorded when the satellite's orbits were near the epicentre of the Earthquake (i.e. areas selected according to Dobrovolsky Formula $R = 10^{0.43M}$ which relates the extend of affected area to the magnitude of the earthquake). With an increase in total ion density observed around 10:30 local time on 25 September, 2009, it was expected that an Earthquake with magnitude between 7 and 8Mw would occur between 26 September and 10 October, 2009 (Figure 4(a)). Also, the changes in electron density showed unusual behaviour. These changes peaked around 10:30 am local time and exceeded 9.77% upper bound on September 25, 2009 (Figure 4(b)). The ion density anomaly was observed around 10:30 local time on September 25, 2009. For $D_x = 2.61$, the magnitude of the impending Earthquake is estimated to be between 7 and 8Mw that would have happened between September 26 and October 10, 2009 (Figure 4(c)). An unusual increase in total ion density was observed around 22:30 local time on September 24, 2009 (Figure 4d). For this anomaly, an Earthquake with magnitude greater than 8Mw would be expected to happen between September 25 and October 9.

By investigating changes in SST, there was sharp increase of 8.03% on September 6, 2009 (Figure 4(g)). The irregularity seen on September 6 indicates that an Earthquake with magnitude between 7 to 8 would have occurred between September 7 and 22.

The AOD obtained from the Aqua sensor shows a maximum anomaly ($Dx = 2.96$) on September 21, 2009 indicating that an Earthquake with magnitude ranging from 7 to 8 Mw would have happened between September 22 and October 7, 2009 (Figure 4h).

The characteristics of detected anomalies using SVR and Random Forest methods are shown in Table 7 and 8, respectively.

In order to finalize each Earthquake's date and magnitude parameters using the parameters obtained from different precursors, the MSE fusion method has been applied. In the case study of Samoa, according to the MSE method, it was predicted that an Earthquake with magnitude between 7 and 8 Mw would occur between September 25 and October 9, 2009 indicated by both Median and SVR results (Table 15). Based on Random Forest method, the parameters would happen between September 20 and October 4, 2009, with magnitude between 7 and 8 Mw.

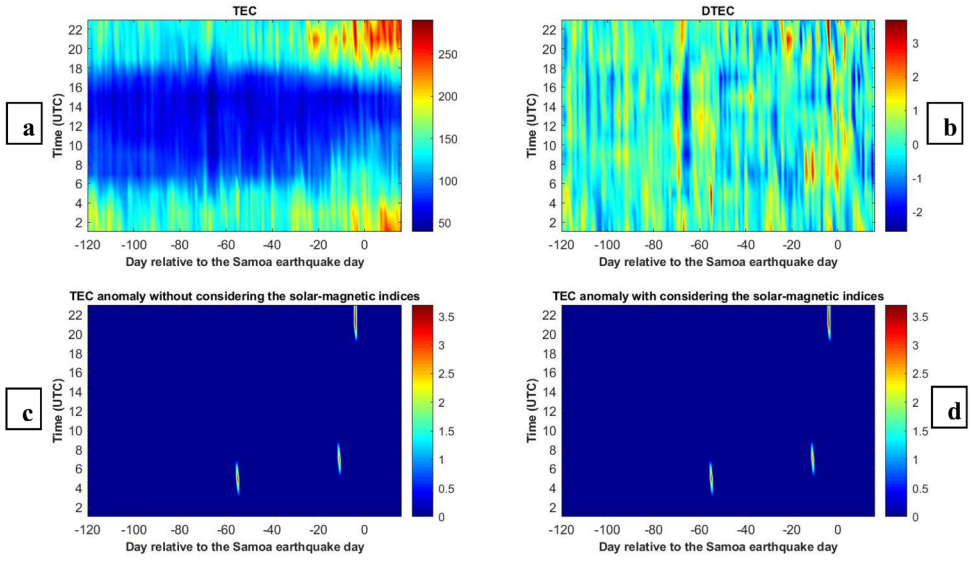

Figure 3. Results of TEC Analysis using median for Samoa earthquake. The earthquake time is indicated by an asterisk. (a) TEC variations, (b) DTEC, (c) Detected anomalies without considering the solar-magnetic indices, (d) Detected anomalies with considering the solar-magnetic indices.

Table 6. List of anomalies obtained from different precursors of the Samoa Earthquake using Median metho

Precursor	Date of observed anomaly	Prediction of earthquake date	Deviation value (Dx)	Prediction of earthquake magnitude (Mw)
Total Ion Density (Day Time)	25 Sep	26 Sep-10 Oct	2.86	7<Mw<8
Electron Density (Day Time)	25 Sep	26 Sep-10 Oct	2.63	7<Mw<8
Ion Density (Day Time)	25 Sep	26 Sep-10 Oct	2.61	7<Mw<8
Total Ion Density (Night Time)	24 Sep	25 Sep-9 Oct	4.58	Mw>8
Electron Density (Night Time)	24 Sep	25 Sep-9 Oct	3.00	Mw>8
Ion Density (Night Time)	24 Sep	25 Sep-9 Oct	3.51	Mw>8
Total Ion Density (Night Time)	5 Sep	6 Sep-20 Sep	2.85	7<Mw<8
TEC	25 Sep (UTC=24:00)	26 Sep-10 Oct	3.18	Mw>8
	25 Sep (UTC=22:00)	26 Sep-10 Oct	3.70	Mw>8
	18 Sep (UTC=08:00)	19 Sep-3 Oct	3.10	Mw>8
Sea Surface Temperature	6 Sep	7 Sep-22 Sep	2.70	7<Mw<8
Aerosol Optical Depth (Aqua)	21 Sep	22 Sep-7 Oct	2.96	7<Mw<8

Table 7. List of anomalies obtained from different precursors of the Samoa earthquake using SVR method

Precursor	Date of observed anomaly	Prediction of earthquake date	Deviation value (Dx)	Prediction of earthquake magnitude (Mw)
Total Ion Density (Day Time)	25 Sep	26 Sep-10 Oct	2.76	7<Mw<8
Electron Density (Day Time)	25 Sep	26 Sep-10 Oct	2.25	7<Mw<8
Ion Density (Day Time)	25 Sep	26 Sep-10 Oct	2.20	7<Mw<8
Total Ion Density (Night Time)	24 Sep	25 Sep-9 Oct	2.57	7<Mw<8
Electron Density (Night Time)	24 Sep	25 Sep-9 Oct	2.53	7<Mw<8
Ion Density (Night Time)	24 Sep	25 Sep-9 Oct	2.54	7<Mw<8
TEC	28 Sep (UTC=14:00)	29 Sep-13 Oct	-2.53	7<Mw<8
	20 Sep (UTC=16:00)	21 Sep-5 Oct	-2.59	7<Mw<8
	17 Sep (UTC=22:00)	18 Sep-2 Oct	2.93	7<Mw<8
	13 Sep (UTC=14:00)	14 Sep-28 Sep	2.51	7<Mw<8
	7 Sep (UTC=08:00)	8 Sep-22 Sep	2.80	7<Mw<8
Sea Surface Temperature	6 Sep	7 Sep-22 Sep	3.80	Mw>8
Aerosol Optical Depth (Aqua)	21 Sep	22 Sep-7 Oct	3.09	Mw>8

Table 8. List of anomalies obtained from different precursors of the Samoa earthquake using Random Forest method

Precursor	Date of observed anomaly	Prediction of earthquake date	Deviation value (Dx)	Prediction of earthquake magnitude (Mw)
Total Ion Density (Day Time)	25 Sep	26 Sep-10 Oct	2.60	7<Mw<8
Electron Density (Day Time)	25 Sep	26 Sep-10 Oct	2.35	7<Mw<8
Ion Density (Day Time)	25 Sep	26 Sep-10 Oct	2.07	7<Mw<8
Ion Density (Night Time)	24 Sep	25 Sep-9 Oct	2.72	7<Mw<8
Electron Density (Night Time)	24 Sep	25 Sep-9 Oct	2.65	7<Mw<8
Total Ion Density (Day Time)	24 Sep	25 Sep-9 Oct	2.52	7<Mw<8
TEC	19 Sep (UTC=14:00)	20 Sep-4 Oct	2.63	7<Mw<8
	17 Sep (UTC=22:00)	18 Sep-2 Oct	2.81	7<Mw<8
	17 Sep (UTC=16:00)	18 Sep-2 Oct	-2.54	7<Mw<8
	13 Sep (UTC=12:00)	14 Sep-28Sep	2.71	7<Mw<8
	7 Sep (UTC=10:00)	8 Sep-22 Sep	2.54	7<Mw<8
	7 Sep (UTC=08:00)	8 Sep-22 Sep	2.70	7<Mw<8
Sea Surface Temperature	9 Sep	10 Sep-25 Sep	-2.75	7<Mw<8
	6 Sep	7 Sep-22 Sep	3.20	Mw>8
Aerosol Optical Depth (Aqua)	21 Sep	22 Sep-7 Oct	3.52	Mw>8

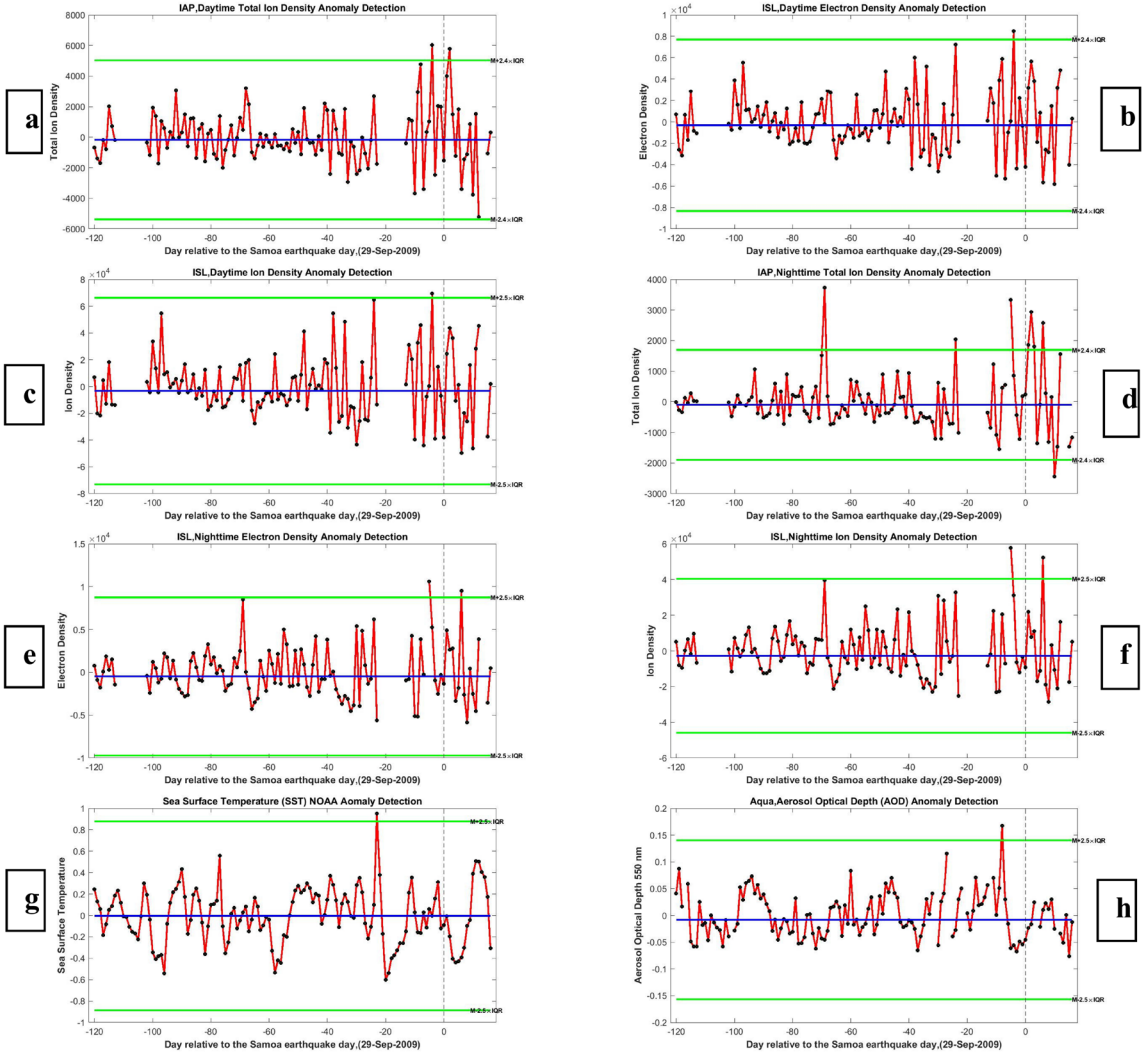

Figure 4. Results of (a) Daytime total ion density data (IAP, DEMETER), (b) Daytime electron density data (ISL, DEMETER), (c) Daytime ion density data (ISL, DEMETER), (d) Night-time total density data (IAP, DEMETER), (e) Night-time electron density data (ISL, DEMETER), (f) Night-time ion density data (ISL, DEMETER), (g) SST (NOAA), (h) AOD data (Aqua, MODIS), analysis using median method for Samoa earthquake.

Sichuan earthquake

In the case study of Sichuan Earthquake, all time series data were provided for the period of 1 February to 27 May 2008. Some intense anomalies related to TEC data have been observed on April 5 (2 UTC), and May 9 (14 UTC) (Figure 5(d)). These strong anomalies indicate an impending Earthquake with magnitude between 7 and 8 Mw.

The variations of the various parameters extracted from the DEMETER experimental data over the Sichuan region have been presented in Table 9. A sudden and unusual change in total ion density has been observed three days prior to the Earthquake around 22:30 local time (Figure 6(a)). This means that an Earthquake with magnitude ranging from 7 to 8 Mw would have occurred between May 3 and 7, 2008. An anomaly has also been observed on May 3, 2008 in electron density around 10:30 local time which implies an impending earthquake as strong as 7 to 8 Mw between 4 April and 18 May (Figure 6(b)). An unusual decrease have been observed in ion temperature around 10:30 local time on May 3, 2008 (Figure 6(c)). The characteristics of other detected anomalies are seen in Table 9.

The Tables 10 and 11 show the result of anomaly detection by SVR and Random Forest methods, respectively.

By using the MSE method and the combination of the earthquake parameters obtained from different precursors, it was predicted that an earthquake $7<Mw<8$ would have happened between 8 and 22 May 2008 (Table 15). Also, the MSE method for Random Forest and SVR methods indicate that an Earthquake with the magnitude between 7 to 8 Mw would have been occurred between 3 and 17 May, 2008 (Table 15).

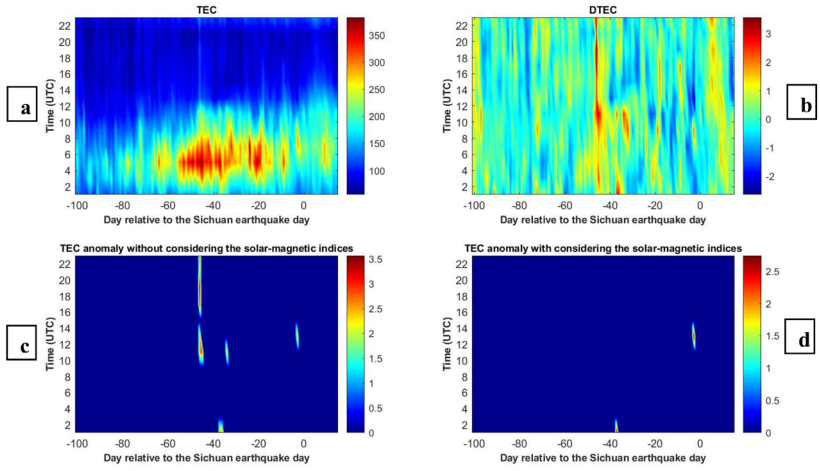

Figure 5. Results of TEC Analysis using median for Sichuan earthquake. The earthquake time is indicated by an asterisk. (a) TEC variations, (b) DTEC, (c) Detected anomalies without considering the solar-magnetic indices, (d) Detected anomalies with considering the solar-magnetic indices.

Table 9. List of anomalies obtained from different precursors of the Sichuan Earthquake using Median method

Precursor	Date of observed anomaly	Prediction of earthquake date	Deviation value (Dx)	Prediction of earthquake magnitude (Mw)
Electron Density (Day Time)	3 May	4 May-18 May	2.45	7<Mw<8
Ion Temperature (Day Time)	3 May	4 May-18 May	-1.90	6<Mw<7
Total Ion Density (Night Time)	2 May	3 May-17 May	2.60	7<Mw<8
TEC	9 May(UTC=14:00)	10 May-24 May	-2.65	7<Mw<8
	5 May (UTC=02:00)	6 May-20 May	2.74	7<Mw<8
LST Aqua (Night Time)	3 May	4 May-19 May	-4.89	Mw>8
Aerosol Optical Depth (Aqua)	9 May	10 May-25 May	2.76	7<Mw<8
SLHF	11 May	12 May-27 May	2.06	7<Mw<8

Table 10. List of anomalies obtained from different precursors of the Sichuan Earthquake using SVR method

Precursor	Date of observed anomaly	Prediction of earthquake date	Deviation value (Dx)	Prediction of earthquake magnitude (Mw)
Electron Density (Day Time)	3 May	4 May-18 May	2.76	7<Mw<8
Ion Temperature (Day Time)	3 May	4 May-18 May	-2.27	7<Mw<8
Total Ion Density (Night Time)	2 May	3 May-17 May	1.86	6<Mw<7
Electron Density (Day Time)	21 Apr	22 Apr-6 May	2.55	7<Mw<8
TEC	11 May(UTC=20:00)	12 May-26 May	2.57	7<Mw<8
	2 May(UTC=10:00)	3 May-17 May	2.75	7<Mw<8
	26 Apr (UTC=06:00)	27 Apr-11 May	2.57	7<Mw<8
	26 Apr (UTC=04:00)	27 Apr-11 May	2.99	7<Mw<8
	14 Apr (UTC=04:00)	15 Apr-29 May	3.09	Mw>8
	11 Apr (UTC=08:00)	12 Apr-26 May	2.97	7<Mw<8
	11 Apr (UTC=06:00)	12 Apr-26 May	2.73	7<Mw<8
LST Aqua (Night Time)	3 May	4 May-19 May	-3.97	Mw>8
Aerosol Optical Depth (Aqua)	9 May	10 May-25 May	2.96	7<Mw<8
SLHF	18 Apr	19 May-4 May	2.46	7<Mw<8

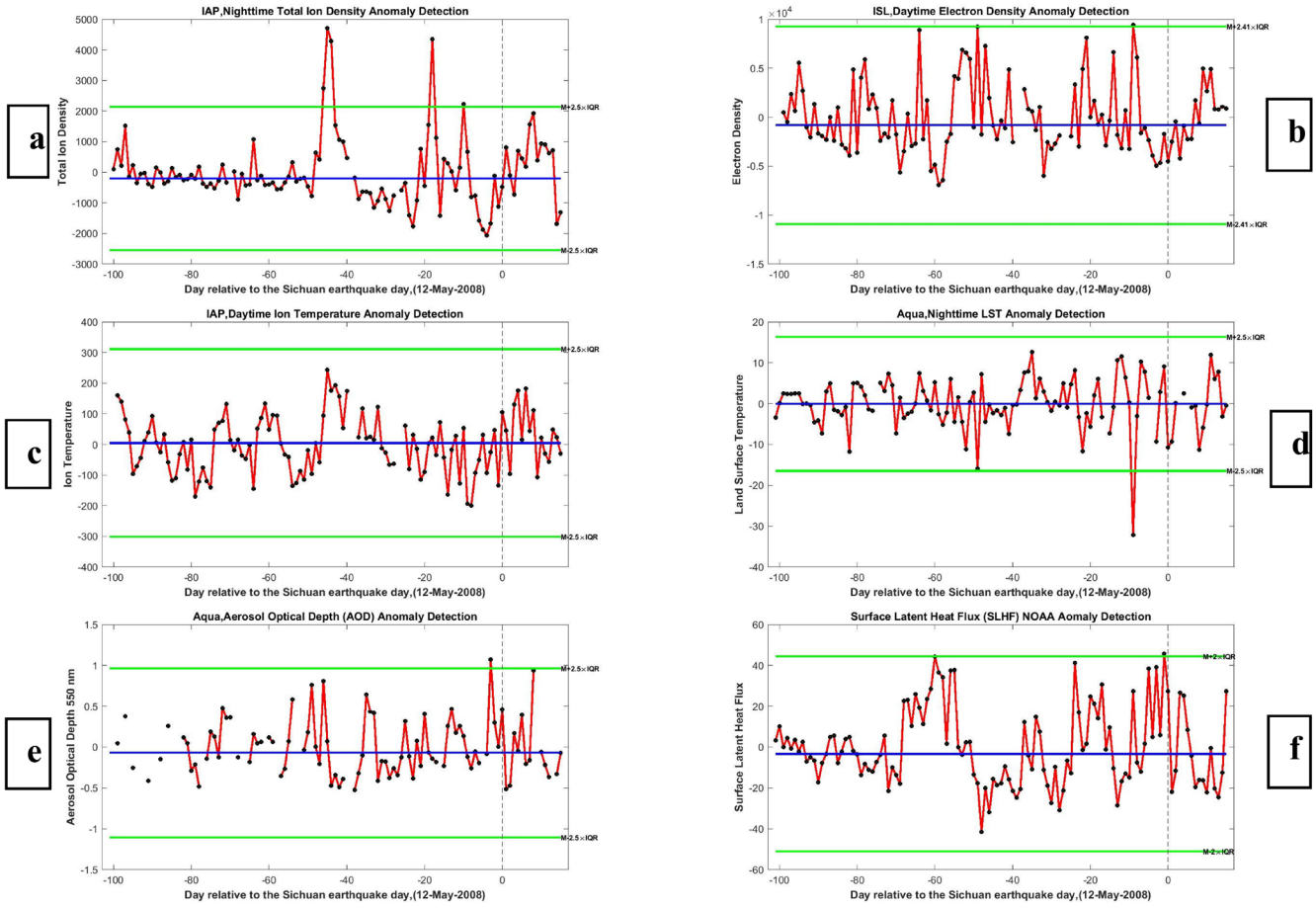

Figure 6. Results of (a) Night-time total ion density data (IAP, DEMETER), (b) Daytime electron density data (ISL, DEMETER), (c) Daytime ion temperature data (IAP, DEMETER), (d) Night-time LST data (Aqua, MODIS), (e) AOD (Aqua, MODIS), (f) SLHF (NOAA), analysis using median method for Sichuan earthquake.

Table 11. List of anomalies obtained from different precursors of the Sichuan Earthquake using Random Forest method

Precursor	Date of observed anomaly	Prediction of earthquake date	Deviation value (Dx)	Prediction of earthquake magnitude (Mw)
Electron Density (Day Time)	3 May	4 May-18 May	2.76	7<Mw<8
Ion Temperature (Day Time)	3 May	4 May-18 May	-2.27	7<Mw<8
Total Ion Density (Night Time)	2 May	3 May-17 May	1.86	6<Mw<7
TEC	9 May(UTC=10:00)	10 May-24 May	3.40	Mw>8
	3 May (UTC=04:00)	4 May-18 May	2.56	7<Mw<8
	3 May (UTC=18:00)	4 May-18 May	2.39	7<Mw<8
	21 Apr (UTC=04:00)	22 Apr-6 May	3.18	Mw>8
LST Aqua (Night Time)	3 May	4 May-19 May	-3.99	Mw>8
Aerosol Optical Depth (Aqua)	9 May	10 May-25 May	2.51	7<Mw<8
SLHF	11 May	12 May-27 May	2.40	7<Mw<8
	9 May	10 May-25 May	2.10	7<Mw<8
	18 Apr	19 May-4 May	2.35	7<Mw<8

Bam earthquake

For Bam earthquake, the time series data of precursors derived during the period of 1 September 2003 to 10 January 2004.The TEC signal fluctuation exceeded the defined bounds on November 8, 2003. This anomaly indicates that an Earthquake with the magnitude between 6 and 7 Mw would have happened (Figure 7(d)).

By investigating the Aqua night-time LST (°C) anomalies, the minimum value of -1.91°C December 18 indicates an earthquake between December 19 and January 3 with 6<Mw<7 would have happened. Also, a sudden decrease in temperature was observed in the night-time LST data (Aqua sensor) on December 13 and 14, which indicates that an Earthquake with magnitude ranging from 7 to 8 Mw would have been occurred. By investigating the day-time LST (Terra and Aqua Sensors) fluctuations, extreme decreases

in temperature on December 12 and 13, 2003. Moreover, by observing the maximum values of 2.39 and 2.12 on December 6 and 7, respectively, it can be concluded that an Earthquake with magnitude between 7 and 8 Mw would have happened between December 7 and 23. Unusual change in day time LST data (Terra-MODIS sensor) with the minimum value (Dx = -3.71) occurred on November 30. Due to this anomaly, an Earthquake with Mw>8 would have been occurred (Figure 8a to 8d).

Unusual AOD changes on December 12, 2003, with values of 4.76 and 3.75 respectively for the Aqua and Terra sensors indicate an Earthquake with a magnitude greater than 8 Mw would have been occurred between December 13 and 28 (Figure 8(e) & (f)). The characteristics of the SLHF detected anomalies are seen in Table 12.

The anomalies obtained by SVR and Random Forest methods, respectively, are shown in tables 13 and 14.

By combining the predicted parameters obtained from different predictors using the MSE method, it is predicted that an Earthquake would occur between December 13 and 28, 2003, for median anomaly detection method. The combination of anomalies obtained from the SVR and Random Forest by using MSE method predicts an Earthquake between December 13 and 28, 2003. The magnitude of this Earthquake is estimated to be 7<Mw<8 for median, SVR and Random Forest methods (Table 15).

Table 12. List of anomalies obtained from different precursors of Bam Earthquake using Median method

Precursor	Date of observed anomaly	Prediction of earthquake date	Deviation value (Dx)	Prediction of earthquake magnitude (Mw)
TEC	8 Nov (UTC=12:00)	9 Nov-23 Nov	-1.99	6<Mw<7
LST Aqua (Night Time)	18 Dec	19 Dec-3 Jan	-1.91	6<Mw<7
LST Aqua (Night Time)	14 Dec	15 Dec-30 Dec	-2.02	7<Mw<8
LST Aqua (Night Time)	13 Dec	14 Dec-29 Dec	-2.22	7<Mw<8
LST Terra (Day Time)	13 Dec	14 Dec-29 Dec	-2.06	7<Mw<8
LST Aqua (Day Time)	13 Dec	14 Dec-29 Dec	-2.46	7<Mw<8
LST Terra (Day Time)	12 Dec	13 Dec-28 Dec	-2.34	7<Mw<8
LST Terra (Night Time)	12 Dec	13 Dec-28 Dec	-2.24	7<Mw<8
LST Aqua (Day Time)	12 Dec	13 Dec-28 Dec	-3.10	Mw>8
LST Terra (Night Time)	7 Dec	8 Dec-23 Dec	2.12	7<Mw<8
LST Aqua (Night Time)	7 Dec	8 Dec-23 Dec	2.09	7<Mw<8
LST Terra (Night Time)	6 Dec	7 Dec-22 Dec	2.39	7<Mw<8
LST Aqua (Night Time)	6 Dec	7 Dec-22 Dec	2.02	7<Mw<8
LST Aqua (Night Time)	5 Dec	6 Dec-21 Dec	2.01	7<Mw<8
LST Terra (Day Time)	30 Nov	1 Dec-16 Dec	-3.71	Mw>8
Aerosol Optical Depth (Aqua)	12 Dec	13 Dec-28 Dec	4.76	Mw>8
Aerosol Optical Depth (Terra)	12 Dec	13 Dec-28 Dec	3.75	Mw>8
SLHF	25 Dec	26 Dec-10 Jan	-3.06	Mw>8
	23 Dec	24 Dec-8 Jan	3.60	Mw>8
	21 Dec	22 Dec-6 Jan	-3.03	Mw>8
	18 Dec	19 Dec-3 Jan	-2.56	7<Mw<8
	15 Dec	16 Dec-31 Dec	5.30	Mw>8
	13 Dec	14 Dec-29 Dec	8.34	Mw>8
	6 Dec	7 Dec-22 Dec	7.51	Mw>8
	5 Dec	6 Dec-21 Dec	4.70	Mw>8
	25 Nov	26 Nov-11 Dec	2.67	7<Mw<8
	24 Nov	25 Nov-10 Dec	3.10	Mw>8

Table 13. List of anomalies obtained from different precursors of the Bam earthquake using SVR method

Precursor	Date of observed anomaly	Prediction of earthquake date	Deviation value (Dx)	Prediction of earthquake magnitude (Mw)
TEC	21 Dec (UTC=10:00)	22 Dec-5 Jan	2.80	7<Mw<8
	21 Dec (UTC=08:00)	22 Dec-5 Jan	2.75	7<Mw<8
LST Aqua (Day Time)	16 Dec	17 Dec-1 Jan	3.26	Mw>8
LST Aqua (Day Time)	12 Dec	13 Dec-28 Dec	-2.71	7<Mw<8
LST Terra (Day Time)	12 Dec	13 Dec-28 Dec	-2.34	7<Mw<8
LST Terra (Night Time)	12 Dec	13 Dec-28 Dec	-2.21	7<Mw<8
LST Terra (Night Time)	5 Dec	6 Dec-21 Dec	2.25	7<Mw<8
LST Aqua (Day Time)	5 Dec	6 Dec-21 Dec	2.16	7<Mw<8
LST Terra (Night Time)	3 Dec	4 Dec-19 Dec	-2.21	7<Mw<8
LST Terra (Day Time)	30 Nov	1 Dec-16 Dec	-3.42	Mw>8
Aerosol Optical Depth (Aqua)	12 Dec	13 Dec-28 Dec	3.788	Mw>8
Aerosol Optical Depth (Terra)	14 Dec	15 Dec-30 Dec	3.74	Mw>8
SLHF	12 Dec	13 Dec-28 Dec	-2.74	7<Mw<8
	13 Dec	14 Dec-29 Dec	2.43	7<Mw<8

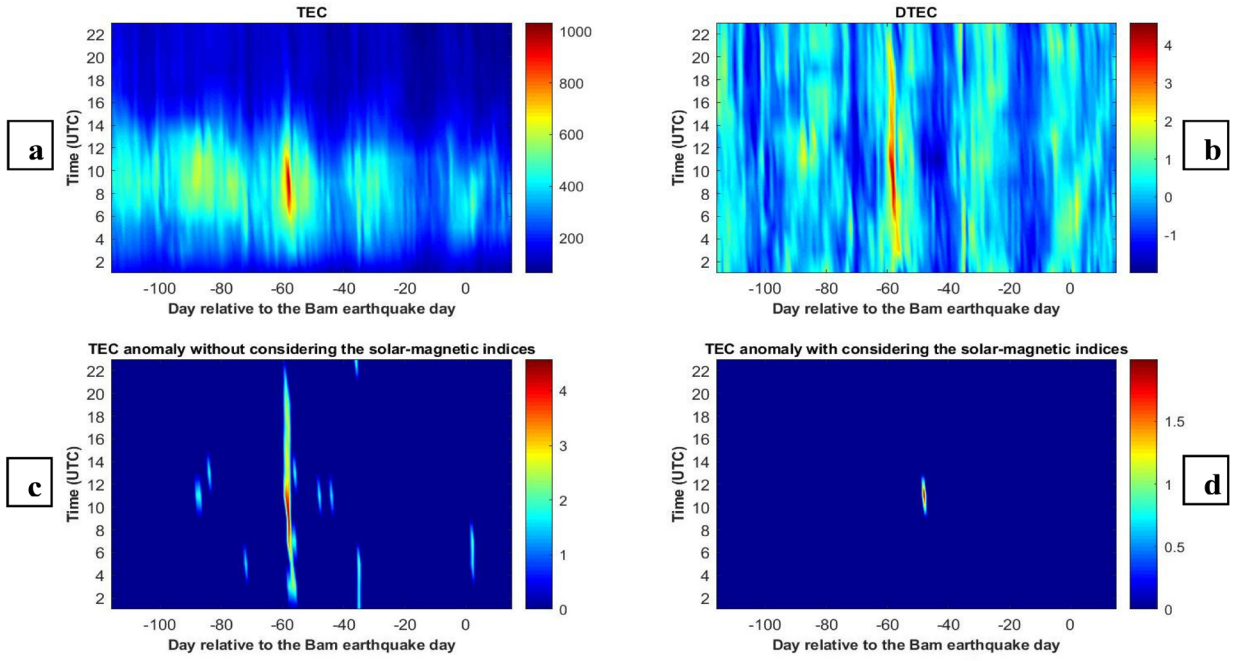

Figure 7. Results of TEC Analysis using median for Bam earthquake. The earthquake time is indicated by an asterisk. (a) TEC variations, (b) DTEC, (c) Detected anomalies without considering the solar-magnetic indices, (d) Detected anomalies with considering the solar-magnetic indices.

Table 14. List of anomalies obtained from different precursors of Bam Earthquake using Random Forest method

Precursor	Date of observed anomaly	Prediction of earthquake date	Deviation value (Dx)	Prediction of earthquake magnitude (Mw)
TEC	23 Dec (UTC=02:00)	24 Dec-7 Jan	-1.92	6<Mw<7
	21 Dec (UTC=10:00)	22 Dec-5 Jan	2.36	7<Mw<8
	21 Dec (UTC=08:00)	22 Dec-5 Jan	2.53	7<Mw<8
	12 Dec (UTC=24:00)	13 Dec-27 Dec	2.27	7<Mw<8
	12 Dec(UTC=22:00)	13 Dec-27 Dec	1.81	6<Mw<7
	10 Dec (UTC=16:00)	11 Dec-25 Dec	1.80	6<Mw<7
LST Terra (Day Time)	13 Dec	14 Dec-29 Dec	-1.94	6<Mw<7
LST Aqua (Day Time)	13 Dec	14 Dec-29 Dec	-2.69	7<Mw<8
LST Terra (Night Time)	12 Dec	13 Dec-28 Dec	-1.92	6<Mw<7
LST Aqua (Day Time)	12 Dec	13 Dec-28 Dec	-3.56	Mw>8
LST Terra (Day Time)	30 Nov	1 Dec-16 Dec	-3.60	Mw>8
Aerosol Optical Depth (Aqua)	12 Dec	13 Dec-28 Dec	4.01	Mw>8
Aerosol Optical Depth (Terra)	12 Dec	13 Dec-28 Dec	3.83	Mw>8
SLHF	13 Dec	14 Dec-29 Dec	2.55	7<Mw<8

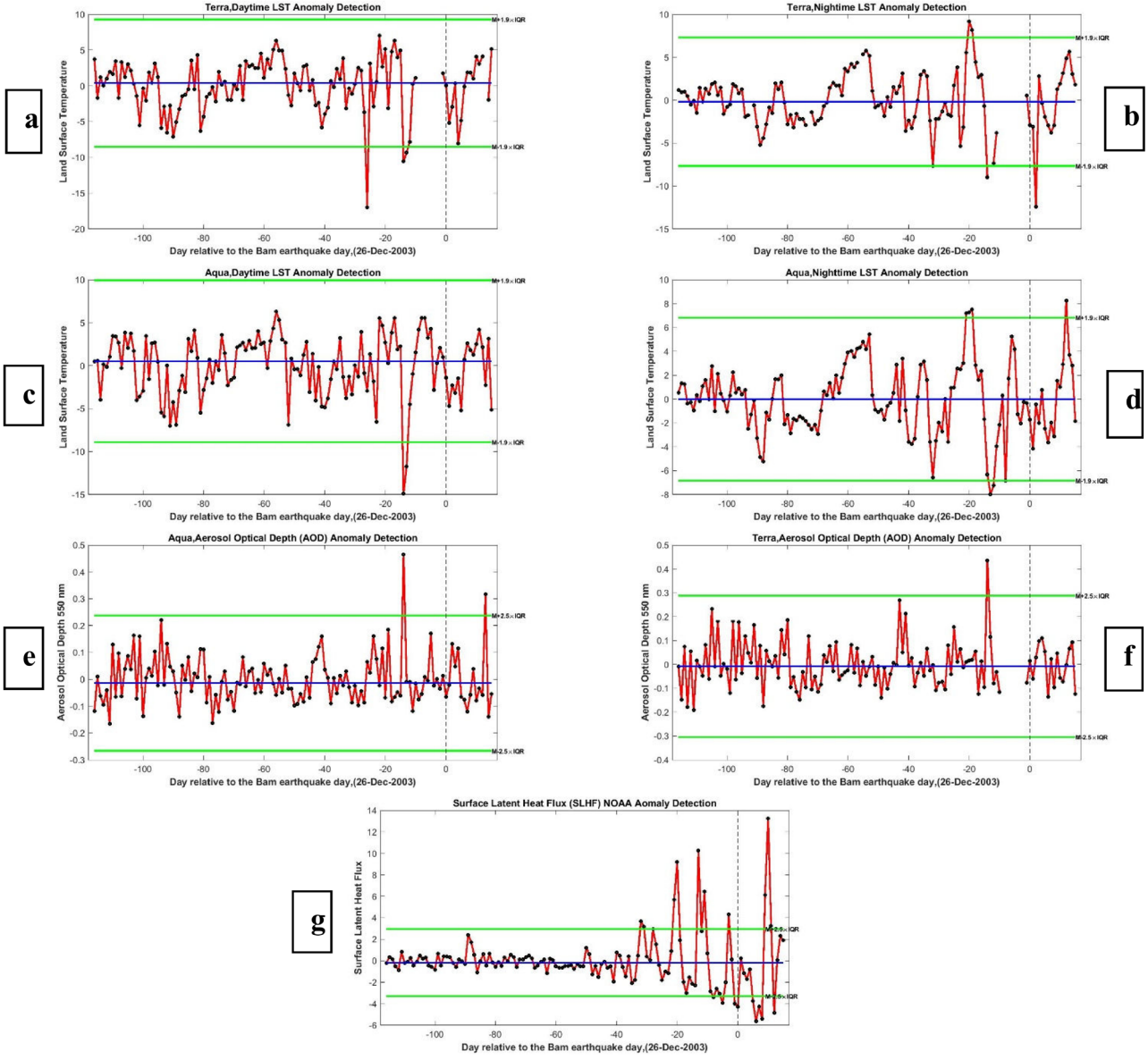

Figure 8. Results of (a) Daytime LST data (Terra, MODIS), (b) Night-time LST data (Terra, MODIS), (c) Daytime LST data (Aqua, MODIS), (d) Night-time LST data (Aqua, MODIS), (e) AOD data (Aqua, MODIS), (f) AOD (Terra, MODIS), (g) SLHF (NOAA), analysis using median method for Bam earthquake.

Table 15. The registered and estimated earthquake parameters related to the case studies

Case Study	Earthquake Date				Earthquake Magnitude (Mw)			
	Registered	Estimated MSE Method			Registered	Estimated MSE Method		
		Median	SVR	RF		Median	SVR	RF
Kermanshah	12 Nov 2017	1-16 Nov 2017	1-16 Nov 2017	29 Oct-12 Nov 2017	7.3	>8	7-8	7-8
Samoa	29 Sep 2009	25 Sep-9 Oct 2009	25 Sep-9 Oct 2009	20 Sep-4 Oct 2009	8.1	7-8	7-8	7-8
Sichuan	12 May 2008	8-22 May 2008	3-17 May 2008	3-17 May 2008	7.9	7-8	7-8	7-8
Bam	26 Dec 2003	13-28 Dec 2003	13-28 Dec 2003	13-28 Dec 2003	6.6	7-8	7-8	7-8

5. Conclusions

Assuming that estimation of Earthquake parameters using each predictor individually is accompanied by some uncertainties, this study considered integrating the capabilities of different earthquake parameters extracted from some of the same earthquake predictors to better estimate earthquake parameters. By using the combination of precursors in this study, the uncertainties in estimating earthquake parameters have been removed implicitly. To identify the anomalous states that may be associated with impending earthquakes, variations of different earthquake precursors have been analysed for four earthquakes by using Median, SVR and Random Forest methods. For each precursor, the date and magnitude were estimated according to the earthquake signals. By integrating the earthquake parameters obtained from all precursors, the final earthquake parameters were estimated more accurately.

Since different precursors have been used to analyse the final earthquake parameters, therefore, for all earthquakes, the estimated earthquake parameters for each earthquake are close to the actually recorded parameters. This can lead to accurate estimation of earthquake parameters with respect to the number and variety of earthquake precursors. Based on the results, it seems that methods such as SVR and Random Forest dealing with nonlinear and complex behaviours of time series are more sensitive than the Median method. Therefore, it can be accounted that these methods are suitable tools for detecting anomalies in nonlinear time series related to changes in seismic precursors.

Since various factors can cause unusual behaviour in different ionospheric, atmospheric or lithospheric parameters, more careful studies should be conducted to distinguish the anomalies caused by the daily changes from anomalies due to seismic activities.

Acknowledgements

The authors would like to acknowledge LPC2E for the DEMETER data, NASA Jet Propulsion Laboratory for the TEC data and NOAA for the geomagnetic indices, SST and SLHF data. Also analyses and visualizations used in this study were produced with the Giovanni online data system, developed and maintained by the NASA GES DISC.

References

Akhoondzadeh, M. (2013). An Adaptive Network-based Fuzzy Inference System for the detection of thermal and TEC anomalies around the time of the Varzeghan, Iran, (Mw D 6.4) earthquake of 11 August 2012. Advances in Space Research, 52(5), 837–852. https://doi.org/10.1016/j.asr.2013.05.024

Akhoondzadeh, M. (2015). Ant Colony Optimization detects anomalous aerosol variations associated with the Chile earthquake of 27 February 2010. Advances in Space Research, 55(7), 1754–1763. https://doi.org/10.1016/j.asr.2015.01.016

Akhoondzadeh, M., De Santis, A., Marchetti, D., Piscini, A., & Cianchini, G. (2018). Multi precursors analysis associated with the powerful Ecuador (MW = 7.8) earthquake of 16 April 2016 using Swarm satellites data in conjunction with other multi-platform satellite and ground data. Advances in Space Research, 61(1), 248–263. https://doi.org/10.1016/j.asr.2017.07.014

Akhoondzadeh, M., De Santis, A., Marchetti, D., Piscini, A., & Jin, S. (2019). Anomalous seismo-LAI variations potentially associated with the 2017 Mw = 7.3 Sarpol-e Zahab (Iran) earthquake from Swarm satellites, GPS-TEC and climatological data. Advances in Space Research, 64, 143–158. https://doi.org/10.1016/j.asr.2019.03.020

Alvan, H.V., Azad, F.H., & Mansor, S. (2013). Latent heat flux and air temperature anomalies along an active fault zone associated with recent Iran earthquakes. Advances in Space Research, 52(9), 1678–1687. https://doi.org/10.1016/j.asr.2013.08.002

Berthelier, J.J., Godefroy, M., Leblanc, F., Seran, E., Peschard, D., Gilbert, P., & Artru, J. (2006). IAP, the thermal plasma analyzer on DEMETER. Planetary and Space Science, 54(5), 487–501. https://doi.org/10.1016/j.pss.2005.10.018

Bhardwaj, A., Singh, S., Sam, L., & Bhardwaj, A. (2017a). Martín-Torres F J, Singh A, Kumar R. MODIS-based estimates of strong snow surface temperature anomaly related to high altitude earthquakes of 2015. Remote Sensing of Environment, 188, 1–8. https://doi.org/10.1016/j.rse.2016.11.005

Bhardwaj, A., Singh, S., Sam, L., Joshi, P.K., Bhardwaj, A., Martín-Torres, F.J., & Kumar, R. (2017b). A review on remotely sensed land surface temperature anomaly as an earthquake precursor. International Journal of Applied Earth Observation and Geoinformation, 63, 158–166. https://doi.org/10.1016/j.jag.2017.08.002

Breiman, L. (2011). Random forests. Machine Learning, 45(1), 5-32. https://doi.org/10.1023/A:1010933404324

Blackett, M., Wooster, M.J., & Malamud, B.D. (2011). Exploring land surface temperature earthquake precursors: A focus on the Gujarat (India) earthquake of 2001. Geophysical Research Letters, 38(15). https://doi.org/10.1029/2011GL048282

Cervone, G., Kafatos, M., Napoletani, D., & Singh, R.P. (2004). Wavelet maxima curves of surface latent heat flux associated with two recent Greek earthquakes. Natural Hazards and Earth System Sciences, 4(3), 359–374. https://doi.org/10.5194/nhess-4-359-2004

Cervone, G., Maekawa, S., Singh, R.P., Hayakawa, M., Kafatos, M., & Shvets, A. (2006). Surface latent heat flux and nighttime LF anomalies prior to the Mw = 8.3 TokachiOki earthquake. Natural Hazards and Earth System Sciences, 6(1), 109–114. https://doi.org/10.5194/nhess-6-109-2006

Chen, S., Xu, Z., Liu, P., Feng, T., Wang, D., Jiao, Z., Chen, L., & Zhang, G. (2020). Exploring Changes in Land Surface Temperature Possibly Associated with Earthquake: Case of the April 2015 Nepal Mw 7.9 Earthquake. Entropy, 22(4), 377-400. https://doi.org/10.3390/e22040377

Cutler, D.R., Edwards, Jr. TC., Beard, K.H., Cutler, A., Hess, K.T., Gibson, J., & Lawler, J.J. (2007). Random forests for classification in ecology. Ecology, 88(11), 2783-2792. https://doi.org/10.1890/07-0539.1

Dey, S., & Singh, R.P. (2003). Surface latent heat flux as an earthquake precursor. Natural Hazards and Earth System Sciences, 3(6), 749–755. https://doi.org/10.5194/nhess-3-749-2003

Dobrovolsky, I.R., Zubkov, S.I., & Myachkin, V.I. (1979). Estimation of the size of earthquake preparation zones. Pure and Applied Geophysics, 117, 1025–1044. https://doi.org/10.1007/BF00876083

Dziak, R.P., Chadwick, W.W., Fox, C.G., & Embley, R.W. (2003). Hydrothermal temperature changes at the southern Juan de Fuca Ridge associated with MW 6.2 Blanco Transform earthquake. Geology, 31(2), 119–122. https://doi.org/10.1130/0091-7613(2003)031<0119:HTCATS>2.0.CO;2

Eleftheriou, A., Filizzola, C., Genzano, N., Lacava, T., Lisi, M., Paciello, R., Pergola, N., Vallianatos, F., & Tramutoli, V. (2016). Longterm RST analysis of anomalous TIR sequences in relation with earthquakes occurred in Greece in the period 2004–2013. Pure and Applied Geophysics, 173(1), 285-303. https://doi.org/10.1007/s00024-015-1116-8

Freund, F.T., Kulahci, I.G., Cyr, G., Ling, J., Winnick, M., Tregloan-Reed, J., & Freund, M.M. (2009). Air ionization at rock surfaces and pre-earthquake signals. Journal of Atmospheric and Solar-Terrestrial Physics, 71(17), 1824–1834. https://doi.org/10.1016/j.jastp.2009.07.013

Ganguly, N.D. (2016). Atmospheric changes observed during April 2015 Nepal earthquake. Journal of Atmospheric and Solar-Terrestrial Physics, 140, 16–22. https://doi.org/10.1016/j.jastp.2016.01.017

Ibanga, J.I., Akpan, A.E., George, N.J., Ekanem, A.M., & George, A.M. (2018). Unusual ionospheric variations before the strong Auckland Islands, New Zealand earthquake of 30th September, 2007. NRIAG Journal of Astronomy and Geophysics, 7 (1), 149–154. https://doi.org/10.1016/j.nrjag.2017.12.007

Jiao, Z.H., & Shan, X. (2021). Statistical framework for the evaluation of earthquake forecasting: A case study based on satellite surface temperature anomalies. Journal of Asian Earth Sciences, 211. https://doi.org/10.1016/j.jseaes.2021.104710

Jiao, Z.H., Zhao, J., & Shan, X. (2018). Pre-seismic anomalies from optical satellite observations: a review. Natural Hazards and Earth System Sciences, 18(4), 1013–1036. https://doi.org/10.5194/nhess-18-1013-2018

Khosravi, I., Jouybari-Moghaddam, Y., & Sarajian, M.R. (2017). The comparison of NN, SVR, LSSVR and ANFIS at modeling meteorological and remotely sensed drought indices over the eastern district of Isfahan, Iran. Natural Hazards, 87(3), 1507-1522. https://doi.org/10.1007/s11069-017-2827-1

Lebreton, J.P., Stverak, S., Travnicek, P., Maksimovic, M., Klinge, D., Merikallio, S., Lagoutte, D., Poirier, B., Blelly, P.L., Kozacek, Z., & Salaquarda, M. (2006). The ISL Langmuir Probe experiment and its data processing onboard DEMETER: scientific objectives, description and first results. Planetary and Space Science, 54(5), 472–486. https://doi.org/10.1016/j.pss.2005.10.017

Li, M., & Parrot, M. (2012). Real time analysis of the ion density measured by the satellite DEMETER in relation with the seismic activity. Natural Hazards and Earth System Sciences, 12(9), 2957–2963. https://doi.org/10.5194/nhess-12-2957-2012

Li, M., & Parrot, M. (2013). Statistical analysis of an ionospheric parameter as a base for earthquake prediction. Journal of geophysical research: Space physics, 118(6), 3731–3739. https://doi.org/10.1002/jgra.50313

Li, M., & Parrot, M. (2018). Statistical analysis of the ionospheric ion density recorded by DEMETER in the epicenter areas of earthquakes as well as in their magnetically conjugate point areas. Advances in Space Research, 61(3), 974–984. https://doi.org/10.1016/j.asr.2017.10.047

Liaw, A., & Wiener, M (2002). Classification and regression by random Forest. R news, 2(3), 18-22.

Liu, J.Y., Chuo, Y.J., Shan, S.J., Tsai, Y.B., Chen, Y.L., Pulinet, S.A., & Yu, S.B. (2004). Pre-earthquake ionospheric anomalies registered by continuous GPS TEC measurements. Annales Geophysicae, 22(5), 1585–1593. https://doi.org/10.5194/angeo-22-1585-2004

MansouriDaneshvar, M.R., Khosravi, M., & Tavousi, T. (2014). Seismic triggering of atmospheric variables prior to the major earthquakes in the Middle East within a 12-year time-period of 2002–2013. Natural Hazards, 74(3), 1539-1553. https://doi.org/10.1007/s11069-014-1266-5

Ouzounov, D., & Freund, F. (2004). Mid-infrared emission prior to strong earthquakes analyzed by remote sensing data. Advances in Space Research, 33(3), 268–273. https://doi.org/10.1016/S0273-1177(03)00486-1

Ouzounov, D., Bryant, N., Logan, T., Pulinets, S., & Taylor, P. (2006). Satellite thermal IR phenomena associated with some of the major earthquakes in 1999–2003. Physics and Chemistry of the Earth, 31(4), 154–163. https://doi.org/10.1016/j.pce.2006.02.036

Ouzounov, D., Liu, D., Chunli, K., Cervone, G., Kafatos, M., & Taylor, P. (2007). Outgoing long wave radiation variability from IR satellite data prior to major earthquakes. Tectonophysics, 431(1), 211–220. https://doi.org/10.1016/j.tecto.2006.05.042

Panda, S.K., Choudhury, S., Saraf, A.K., & Das, J.D. (2007). MODIS land surface temperature data detects thermal anomaly preceding 8 October 2005 Kashmir earthquake. International Journal of Remote Sensing, 28(20), 4587–4596. https://doi.org/10.1080/01431160701244906

Parrot, M., Benoist, D., Berthelier, J.J., Bł˛ecki, J., Chapuis, Y., Colin, F., Elie, F., Fergeau, P., Lagoutte, D., Lefeuvre, F., Legendre, C., Lévêque, M., Pinçon, J.L., Poirier, B., Seran, H.C., & Zamora, P. (2006). The magnetic field experiment IMSC and its data processing onboard DEMETER: scientific objectives, description and first results. Planetary and Space Science, 54(5), 441–455. https://doi.org/10.1016/j.pss.2005.10.015

Pulinets, S.A., Ouzounov, D., Ciraolo, L., Singh, R., Cervone, G., Leyva, A., Dunajecka, M., Karelin, A.Y., Boyarchuk, K.A., & Kotsarenko, A. (2003). Thermal, atmospheric and ionospheric anomalies around the time of the Colima M7.8 earthquake of 21 January 2003. Annales Geophysicae, 24(3), 835–849. https://doi.org/10.5194/angeo-24-835-2006

Pulinets, S., & Ouzounov, D. (2011). Lithosphere–Atmosphere– Ionosphere Coupling (LAIC) model – An unified concept for earthquake precursors validation. Journal of Asian Earth Sciences, 41(4), 371-382. https://doi.org/10.1016/j.jseaes.2010.03.005

Qin, K., Wu, L.X., Ouyang, X.Y., Shen, X.H., & Zheng, S. (2014). Surface latent heat flux anomalies quasi-synchronous with ionospheric disturbances before the 2007 Pu'er earthquake in China. Advances in Space Research, 53(2), 266–271. https://doi.org/10.1016/j.asr.2013.11.004

Rawat, V., Saraf, A.K., Das, J., Sharma, K., & Shujat, Y. (2011). Anomalous land surface temperature and outgoing long-wave radiation observations prior to earthquakes in India and Romania. Natural Hazards, 59(1), 33–46. https://doi.org/10.1007/s11069-011-9736-5

Saraf, A.K., Rawat, V., Banerjee, P., Choudhury, S., Panda, S.K., Dasgupta, S., & Das, J.D. (2008). Satellite detection of earthquake thermal infrared precursors in Iran. Natural Hazards, 47(1), 119–135. https://doi.org/10.1007/s11069-007-9201-7

Saradjian, M.R., & Akhoondzadeh, M. (2011). Prediction of the date, magnitude and affected area of impending strong earthquakes using integration of multi precursors earthquake parameters. Natural Hazards and Earth System Sciences, 11(4), 1109–1119. https://doi.org/10.5194/nhess-11-1109-2011

Tao, D., Cao, J., Battiston, R., Li, L., Ma, Y., Lie, W., Zima, Z., Wand, L., & Dunlop, M.W. (2017). Seismo-ionospheric anomalies in ionospheric TEC and plasma density before the 17 July 2006 M7.7 south of Java earthquake. Annales Geophysicae, 35(3), 589–598. https://doi.org/10.5194/angeo-35-589-2017

Tronin, A.A. (2006). Remote sensing and earthquakes: A review. Physics and Chemistry of the Earth, 31(4), 138–142. https://doi.org/10.1016/j.pce.2006.02.024

Wackerly, D., Mendenhall, W., & Scheaffer, R.L. (2008). Mathematical Statistics with Applications (7th ed.). Belmont, CA, USA: Thomson Higher Education.

Zoran, M. (2012). MODIS and NOAA-AVHRR l and surface temperature data detect a thermal anomaly preceding the 11 March 2011 Tohoku earthquake. International Journal of Remote Sensing, 33(21), 6805–6817. https://doi.org/10.1080/01431161.2012.692833

Zhang, W., Zhao, J., Wang, W., Ren, H., Chen, L., & Yan, G. (2013). A preliminary evaluation of surface latent heat flux as an earthquake precursor. Natural Hazards and Earth System Sciences, 13(10), 2639–2647. https://doi.org/10.5194/nhess-13-2639-2013